Simulation of natural radioactivity backgrounds in the JUNO central detector *

Xin-Ying Li(李新颖)[1,2] Zi-Yan Deng(邓子艳)[2] Liang-Jian Wen(温良剑)[4] Wei-Dong Li(李卫东)[2]
Zheng-Yun You(尤郑昀)[3] Chun-Xu Yu(喻纯旭)[1] Yu-Mei Zhang(张玉美)[3] Tao Lin(林韬)[2]

[1] School of Physics, Nankai University, Tianjin 300071, China
[2] Institute of High Energy Physics, Chinese Academy of Sciences, Beijing 100049, China
[3] Sun Yat-sen University, Guangzhou 510275, China
[4] State Key Laboratory of Particle Detection and Electronics, Institute of High Energy Physics, Chinese Academy of Sciences, Beijing 100049, China

Abstract: The Jiangmen Underground Neutrino Observatory (JUNO) is an experiment proposed to determine the neutrino mass hierarchy and probe the fundamental properties of neutrino oscillation. The JUNO central detector is a spherical liquid scintillator detector with 20 kton fiducial mass. It is required to achieve a $3\%/\sqrt{E(\mathrm{MeV})}$ energy resolution with very low radioactive background, which is a big challenge to the detector design. In order to ensure the detector performance can meet the physics requirements, reliable detector simulation is necessary to provide useful information for the detector design. A simulation study of natural radioactivity backgrounds in the JUNO central detector has been performed to guide the detector design and set requirements for the radio-purity of the detector materials. The accidental background induced by natural radioactivity in the JUNO central detector is 1.1/day. The result is satisfied for the experiment.

Keywords: JUNO, Geant4, natural radioactivity, singles rate

PACS: 29.40.Mc, 29.85.Fj **DOI:** 10.1088/1674-1137/40/2/026001

1 Introduction

JUNO [1], the Jiangmen Underground Neutrino Experiment, is a multipurpose neutrino experiment designed to determine the neutrino mass hierarchy and precisely measure the oscillation parameters by detecting reactor neutrinos from the Yangjiang and Taishan nuclear power plants. It is also intended to observe supernova neutrinos, study atmospheric, solar and geo-neutrinos, and perform exotic searches at JUNO.

JUNO is being constructed in Kaiping, Jiangmen, in Southern China. It is about 53 km away from Yangjiang and Taishan nuclear power plants, both of which are under construction. The planned total thermal power of these reactors is 36 GW. There are no other nuclear power plants within 200 km. In order to suppress the backgrounds induced by cosmic ray muons, the detector is deployed underground with a total overburden of 700 m of rock.

The current JUNO detector design consists of a liquid scintillator (LS) central detector, a water Cherenkov detector and a top tracker. Its layout is shown in Fig. 1. The LS is contained in a spherical vessel, outside which is the support structure. The space between the LS and the water is a buffer area, where the PMTs are placed.

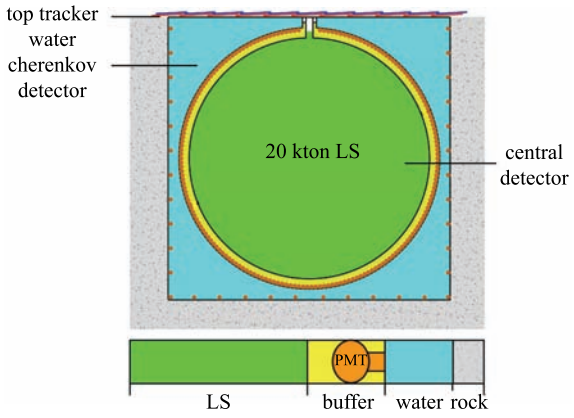

Fig. 1. (color online) A schematic view of the JUNO detector.

Received 13 May 2015, Revised 26 August 2015

∗ Supported by the Strategic Priority Research Program of Chinese Academy of Sciences (XDA10010900), CAS Center for Excellence in Particle Physics (CCEPP), National Natural Science Foundation of China (NSFC), Chinese Academy of Sciences (CAS) Large-Scale Scientific Facility Program, Joint Large-Scale Scientific Facility Funds of NSFC and CAS (U1332201)

1) E-mail: lixy@ihep.ac.cn

In recent years, liquid-scintillator detectors have made important contributions to low-energy neutrino physics [2–7]. The JUNO central detector, with 35.4 m diameter, will be the largest liquid scintillator detector in the world when it is constructed. We use Geant4 [8] simulation to evaluate the design and optimize the dimensions of the detector. Geant4 also has a good ability to simulate the backgrounds induced by the materials.

2 Several options for the central detector

The challenging construction of the JUNO central detector includes the transparent inner tank and the outer supporting structure. To get the energy resolution as good as $3\%/\sqrt{E(\mathrm{MeV})}$, the huge detector has to optimize the collection of optical photons from the liquid-scintillator target while suppressing the variety of background sources.

The collection of optical signals is mainly determined by the light yield and transparency of the LS, and the coverage and quantum efficiency (QE) of the PMT photocathodes. The PMT photocathode coverage should be greater than 75%. In the beginning, there were several design options for the detector: the acrylic option, module option and balloon option. In order to better compare the pros and cons of each option, the PMTs are fixed on the same radius. The PMT coverage is approximately the same in these detector options. The main differences between these detector options lie in the arrangement of the PMTs and the buffer material. In these simulations, the light yield of LS is 10400 photons/MeV, and the QE of PMT is 35%. The attenuation length of LS is 20 m at a wavelength of 430 nm, which corresponds to an absorption length of 60 m with a Rayleigh scattering length of 30 m. Detailed explanations of these options are given in the following subsections.

2.1 Acrylic option

In this option, an acrylic inner tank is spherically shaped to hold 20 ktons of LS. The acrylic sphere is supported by a stainless steel truss while the truss is held by supporting legs at the bottom of the water pool in the experiment hall. To reduce the radioactivity background, oxygen-free copper is used for the joints between the stainless steel truss and acrylic tank. The thickness of the acrylic tank wall is 12 cm. Between the acrylic sphere and the truss, PMTs are mounted inward-facing to the truss to detect the optical signal from the LS. Figure 2 shows the acrylic tank and the steel truss of the central detector. Ultrapure water is added as a shielding liquid outside the acrylic tank.

2.2 Balloon option

In this option the LS container is made of a balloon of nylon or fluoride-rich material, with acrylic board and support structure to hold the balloon, as shown in Fig. 3. The buffer material between the steel tank and nylon balloon is linear alkylbenzene (LAB), which serves as the solvent of the LS. A steel tank holding LS, buffer material and PMTs is placed in the water pool.

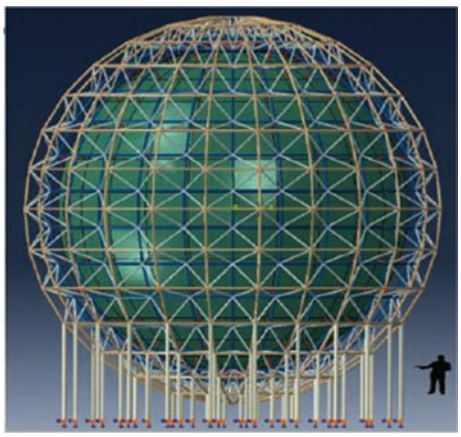

Fig. 2. (color online) Sketch of the acrylic option for the central detector design.

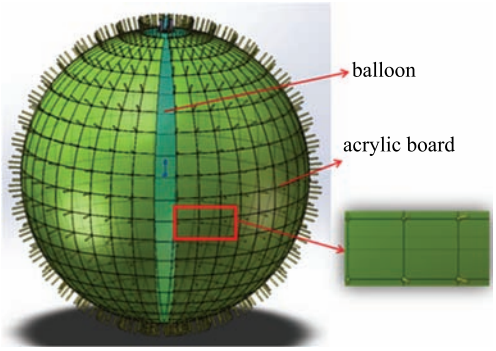

Fig. 3. (color online) Sketch of the balloon option for the central detector design.

2.3 Module option

The module option is proposed to reduce the risk posed by big structures. The modules are made of acrylic. The buffer material and PMTs are placed in the modules. The buffer material is LAB. Two kinds of encapsulations can be taken for different module sizes: small modules with only one PMT in each, or large modules with a set of PMTs in each.

2.3.1 Small module option

In this option, each module is equipped with a single PMT, as shown in Fig. 4, and directly placed in the LS, with buffer material filling up the module. The location of the modules is the same as the PMT arrangement in the acrylic option.

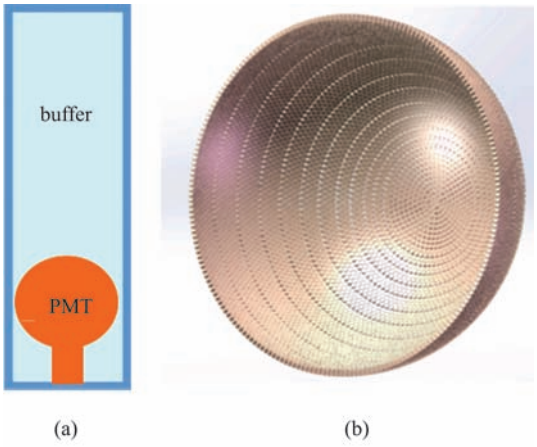

Fig. 4. (color online) The schematics of the small module option. a) The schematic of a small module; b) The small module arrangement in a half sphere.

2.3.2 Large module option

In the large module option, to fill up the whole sphere, the spherical surface is divided into a large number of triangles. First, the surface of the sphere at the radius of the PMT positions is divided into 20 equal parts. Then each part is divided into triangles with ten different kinds of shapes. The sizes of the modules are designed according to the size of the triangles. The numbers of PMTs are different in different modules. A double layer configuration of PMTs has been considered to improve the coverage of PMT.

As shown in Fig. 5, the first layer of the module is filled with closely arrayed PMTs. The number of PMTs in the second layer is less than that in the first one. They are set to fill up the gaps between the PMTs in the first layer. The circles with a number represent the PMTs in the second layer.

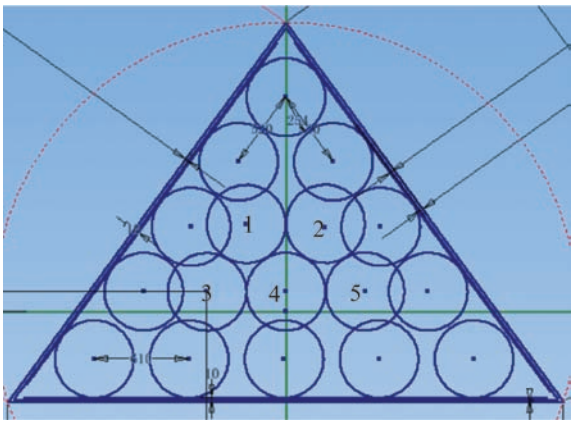

Fig. 5. (color online) PMT arrangement in a large module.

Figure 6 shows the overall arrangement of the large module option using Geant4.

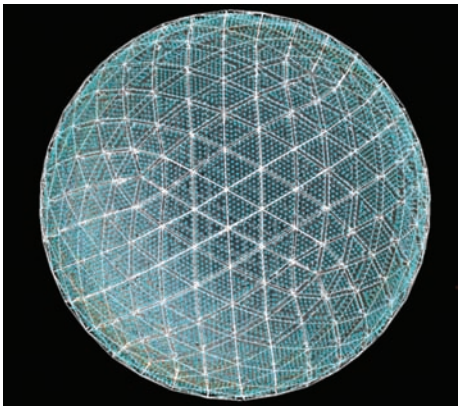

Fig. 6. (color online) The display of all PMTs in the large module option.

3 Comparison of simulation results

The energy spectrum of the backgrounds due to natural radioactive elements overlaps with that of the antineutrino inverse beta decay (IBD). When a combination of two background events meet the selection criteria for IBD, they can form an accidental background and imitate a genuine neutrino event.

The singles rate is an important factor to consider when selecting the detector option. A small singles rate is required for the central detector. In the following, the singles rate means signals from radioactivity depositing >0.7 MeV of visible energy in the LS. Some parameters are set to be consistent in these options, namely the location of the PMTs, the optical parameters of the LS and the thickness of the buffer. We mainly compare the background from PMT glass in each option. The background from PMT glass is mainly due to the radioactive elements (^{238}U, ^{232}Th, ^{40}K). If Schott glass [9] is chosen, the radio-purities of the glass are 22 ppb, 20 ppb and 3.54 ppb, respectively. Figure 7 shows the singles rates from the PMTs in the different options.

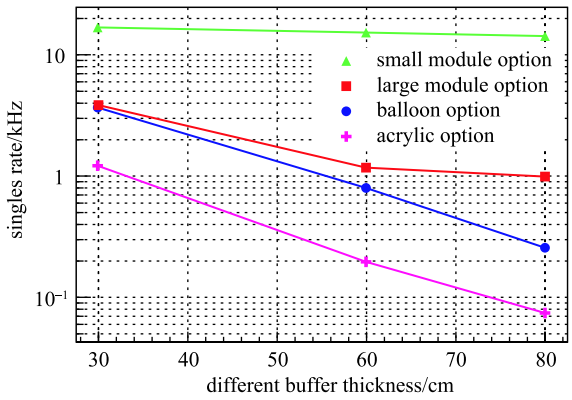

Fig. 7. (color online) Simulation results of the radioactive background rates for different detector options.

The singles rates of the PMTs in the acrylic and balloon options decrease exponentially with the increase of buffer thickness. However, the module options do not show this behaviour, because the gaps of each module are filled with LS. The module option cannot shield the radioactivity background from the PMT glass as well as the other two options. Finally, the module option has been abandoned. Since the acrylic and balloon options are similar, in the following sections we just consider the acrylic option.

4 Research on the acrylic option

Natural radioactivity exists in the materials of the JUNO detector components. In Table 1 and Table 3 the concentrations of primordial nuclides are given as mass fractions (g/g), using the conversion relation for the case of secular equilibrium:

1 ppb = 10^{-9} g/g
1 ppt = 10^{-12} g/g
1 ppb ^{238}U = 12.40 mBq/kg
1 ppb ^{232}Th = 4.05 mBq/kg
1 ppb ^{40}K = 271 mBq/kg

In simulation, the GenDecay package transplanted from the Daya Bay Software System is used as the radioactivity generators. It is assumed that the decay series is in secular equilibrium. The package uses Evaluated Nuclear Structure Data File (ENSDF)[10] to get the decay particles, half-lives and branching ratios.

4.1 Radioactivity of inner materials

The materials of the central detector in the acrylic option mainly include LS, acrylic, oxygen-free copper and stainless steel, as well as the glass of the PMTs. Based on experience [11–13] from the existing neutrino experiments, the specification for the radioactivity of detector materials are listed in Table 1. The buffer thickness in front of the PMT determines the singles rate from the PMTs, so it needs to be optimized by varying the thickness of water in our simulation. The singles rate of the PMTs is nearly 3 Hz when the water thickness is about 1.426 m. LS radius is 17.7 m. Acrylic thickness is 12 cm. The radius of the sphere where the center of PMTs is located is 19.5 m.

External radioactivity can be rejected by a proper fiducial volume cut since their energy deposits are mainly at the LS edge. Thus, the internal LS radio-purity is very important for the JUNO experiment and should be well controlled. The fractional distillation process at the last step of raw LAB production and water extraction of the fluor are necessary to improve the radio-purity of raw LS materials. There will be nitrogen protection during LS production, in order to suppress radon contamination. However, the residual radon contamination will lead to production of the unstable isotope ^{210}Pb (and the subsequent ^{210}Bi decay) which has a half life of 22 years. In the JUNO experiment, the initial purity level of LS that can be achieved without distillation is shown in Table 1. After setting up the on-line distillation, we believe a better purity level with an improvement of two orders of magnitude can be achieved: 10^{-17} g/g for ^{238}U/^{232}Th, 10^{-18} g/g for ^{40}K and 10^{-24} g/g for ^{210}Pb. In this work, the purity level of LS is set to the value without distillation.

Full Monte Carlo simulation is performed to obtain the singles rates from LS and other detector construction materials. The singles rates with different fiducial volume cuts are listed in Table 2.

Table 1. Assumed concentrations of radioactive impurities in different detector materials.

	^{238}U	^{232}Th	^{40}K	^{210}Pb	^{85}Kr	^{39}Ar	^{60}Co
LS	10^{-6} ppb	10^{-6} ppb	10^{-7} ppb	$1.4\cdot10^{-13}$ ppb	50 μBq/m^3	50 μBq/m^3	–
glass	22 ppb	20 ppb	3.54 ppb	–	–	–	–
acrylic	10 ppt	10 ppt	10 ppt	–	–	–	–
steel	1.2 mBq/kg	8.0 mBq/kg	13.4 mBq/kg	–	–	–	2.0 mBq/kg
copper	1.23 mBq/kg	0.405 mBq/kg	0.0377 mBq/kg	–	–	–	–

Table 2. The inner singles rates ($E > 0.7$ MeV) in different fiducial volumes.

fiducial cut/m	LS/Hz	glass/Hz	acrylic/Hz	steel/Hz	copper/Hz	sum/Hz
$R < 17.7$	2.39	2.43	69.23	0.89	0.82	75.76
$R < 17.6$	2.35	1.91	41.27	0.66	0.55	46.74
$R < 17.5$	2.31	1.03	21.82	0.28	0.32	25.76
$R < 17.4$	2.27	0.75	12.23	0.22	0.19	15.66
$R < 17.3$	2.24	0.39	6.47	0.13	0.12	9.35
$R < 17.2$	2.20	0.33	3.61	0.083	0.087	6.31
$R < 17.1$	2.16	0.23	1.96	0.060	0.060	4.47
$R < 17.0$	2.12	0.15	0.97	0.009	0.031	3.28

4.2 Radioactivity from water and rock

The natural radioactivity in the detector surroundings mainly comes from water and rock.

In this work, we have only considered the ^{222}Rn in water. The assumed concentrations of radioactive impurity in water and rock are shown in Table 3.

Table 3. Assumed concentrations of radioactive impurity in water and rock.

water	rock		
^{222}Rn	^{238}U	^{232}Th	^{40}K
0.2 Bq/m^3	10 ppm	30 ppm	5 ppm

4.2.1 ^{222}Rn in water

In an underground laboratory, radon concentration will reach an equilibrium when the decay balances with the emanation from the rock. Radon is soluble in water. The radon concentration in water is nearly 25% of that in air at room temperature. The circulation of water could bring radon into the detector. When the radon concentration in air is 50 Bq/m^3, its concentration in water is assumed to be equally 12.5 Bq/m^3. The singles rate of ^{222}Rn in water is so large that some methods should be taken to reduce the concentration of ^{222}Rn in water. If the concentration can be limited to 0.2 Bq/m^3, with a good N_2 seal and sufficient anti-Rn liner on the water pool walls, then the singles rate is nearly 1.3 Hz when the fiducial volume is 17.2 m.

4.2.2 Rock background

We assume that the radioactivity of rock at the JUNO experiment site is similar to that measured at the Daya Bay site: 10 ppm for ^{238}U, 30 ppm for ^{223}Th and 5 ppm for ^{40}K. Since a full Monte Carlo simulation would be extremely time consuming, a numerical calculation is performed to estimate the effect of the rock radioactivity.

In this method, 50 cm of rock around the water pool is divided into many small parts. The singles rate of each small part is then calculated separately. There are five steps involved in each calculation.

1) Calculate each small part's mass to obtain the initial event rate.
2) Calculate the total event rate of γs (betas are not counted because they cannot travel through water). The ratio of γs is found from simulation. Take ^{232}Th, for instance. There are 665797 γs from 10^6 decays, as illustrated in Fig. 8.
3) Calculate the γ event rate at each energy point ($R_{\rm E}$). The ratio of γ versus energy is also obtained from simulation. In the case of ^{232}Th, this is shown in Fig. 8.
4) The effective solid angle ($\Omega_{\rm eff}$) of each voxel to the LS detector is calculated by taking into account the attenuation of different water thickness.

$$\Omega_{\rm eff} = \sum_{\rm i} \left(\frac{\Delta s_{\rm i} \cos\alpha_{\rm i}}{L_{\rm i}^2} \cdot {\rm e}^{-L_{\rm i} \cdot A_{\rm w}} \right) / 4\pi. \quad (1)$$

As shown in Fig. 9, the surface is divided into many small parts. $\alpha_{\rm i}$ is the angle between the short dashed line and long dashed line. $\beta_{\rm i}$ is the angle between the long dashed line and the thick solid line. $L_{\rm i}$ is the distance between the rock and the detector at different angles. D is the minimum distance between the rock and the central detector. $A_{\rm w}$ is the attenuation coefficient of water at different energies and water thickness.

$$\Delta s_{\rm i} = 2\pi R^2 \cdot \sin\beta_{\rm i} \cdot \Delta\beta, \quad (2)$$

5) Calculate the event rates of each small part after attenuation.

$$R_{\rm parts} = \sum_{E} R_E \cdot \Omega_{\rm eff} \cdot R(E), \quad (3)$$

$$R(E) = {\rm e}^{-L_{\rm r} A_{\rm r}}, \quad (4)$$

$R(E)$ is the attenuation in rock, $A_{\rm r}$ is the attenuation coefficient of rock at different energies, and $L_{\rm r}$ is the attenuation length of γ in rock.

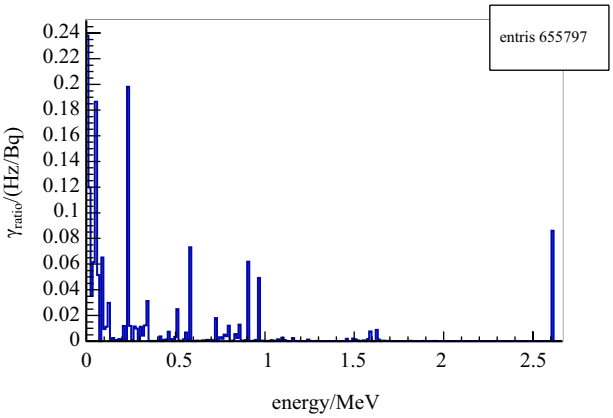

Fig. 8. (color online) $\gamma_{\rm ratio}$ versus energy. $\gamma_{\rm ratio}$ is the ratio of the γ event rate in (Hz) with different energies of γ to the decay rate of the ^{232}Th chain in (Bq).

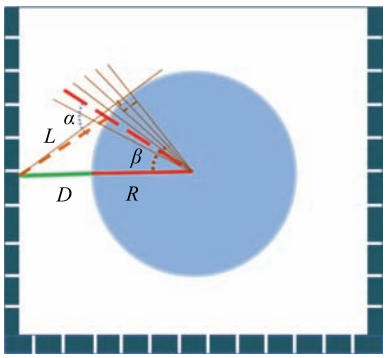

Fig. 9. (color online) Schematic of the variables used in numerical calculation.

In this empirical calculation, the attenuation coefficients are very important. In order to get the attenuation coefficients, a simple model is simulated. In this model, each different energy γ penetrates materials of different thickness vertically. The initial number of γ is $N_{\rm init}$, and the thickness of material is L. $N_{\rm rec}$ is the number of γs with energy greater than 0.7 MeV after passing through the materials. Then, we can calculate the attenuation coefficients with the formula below.

$$A_{\rm w} = -\ln(N_{\rm rec}/N_{\rm init})/L. \quad (5)$$

As shown in Fig. 10, we get the coefficients of each different energy in the case of different thicknesses of water.

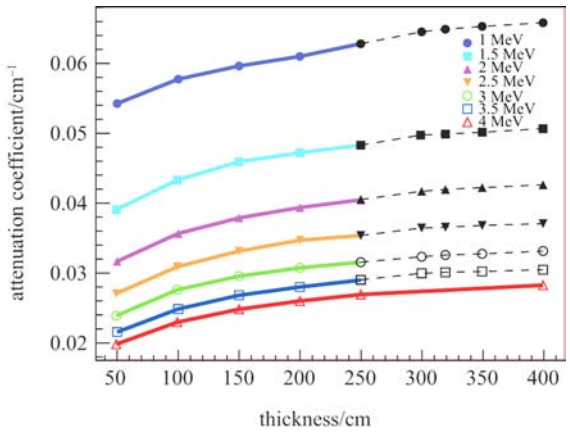

Fig. 10. (color online) Attenuation coefficients of γ in Eq. (1) with different energies in different thicknesses of water. The different marker styles represent different energies. The dashed lines are estimated by the extrapolation method, assuming that the coefficient ratios between different energies are fixed.

We use an extrapolation method to calculate the attenuation coefficients when the thickness is greater than 2.5 m, because it is difficult to get these coefficients in simulation. With these attenuation coefficients we can calculate the final singles rates in different water thicknesses. A real simulation has been performed to verify the validity of the estimation method. In this simulation, the rock thickness is set to be the same as that used in the estimation, and the water thicknesses are 2 m and 2.5 m.

A comparison of simulation and estimation is shown in Table 4. We can tell from the comparison that the estimation is similar to the simulation results. Thus this method can be used to calculate the singles rate of rock. The singles rates of ^{40}K/^{232}Th/^{238}U are estimated to be 0.0742 Hz, 6.739 Hz, 0.613 Hz, respectively, when the thickness of water is 3.2 m. These results satisfy the requirements for the JUNO experiment.

Table 4. Comparison of the results between simulation and estimation with different water thickness.

		simulation/Hz	estimation/Hz
2 m water	^{40}K	161.2	68.9
	^{232}Th	981.0	829.5
	^{238}U	162.2	154.1
2.5 m water	^{40}K	9.0	4.9
	^{232}Th	143.2	133.8
	^{238}U	35.6	17.6

4.3 Accidental background from natural radioactivity

The sum singles rates with different fiducial volume cuts are displayed in Table 5. Based on this table, the radius of the fiducial volume is set to 17.2 m. The total singles rate is 8.6 Hz.

Table 5. The sum singles rates ($E > 0.7$ MeV) with different fiducial volume cuts.

singles rate/Hz	detector components	water	rock	sum
$R < 17.7$ m	75.76	15.94	7.42	99.12
$R < 17.6$ m	46.74	11.00	4.47	62.21
$R < 17.5$ m	25.76	6.58	2.90	35.24
$R < 17.4$ m	15.66	3.84	2.02	21.52
$R < 17.3$ m	9.35	2.20	1.41	12.96
$R < 17.2$ m	6.31	1.31	0.98	8.60
$R < 17.1$ m	4.47	0.78	0.68	5.93
$R < 17.0$ m	3.28	0.46	0.42	4.16

Based on simulation of natural radioactivity background from different detector materials, we can get the scatterplot of the deposited energy of radioactivity background versus LS radius, as shown in Fig. 11. With this scatterplot we can calculate the number of accidental background events for the fiducial volume.

According to the singles rate, a random sample of some background events were generated based on the

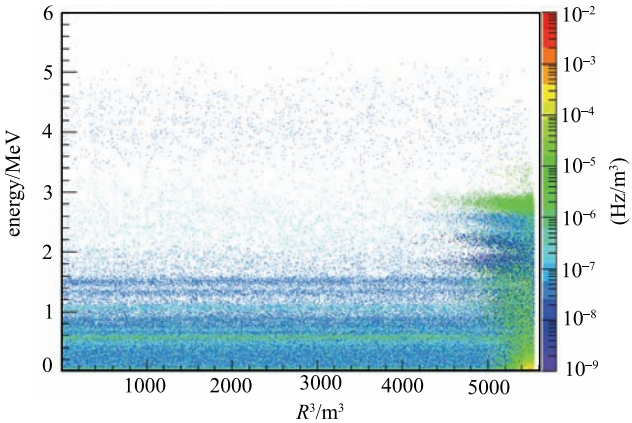

Fig. 11. (color online) Scatterplot of deposited energy versus LS radius.

scatterplot. Then, certain events meeting the criteria listed below were selected.

1) prompt energy cut 0.7 MeV $<E_{\rm p}<$ 12 MeV;
2) delayed energy cut 1.9 MeV $< E_{\rm d} <$ 2.5 MeV;
3) time difference between the prompt and delayed signal: 1.0 μs $< \Delta T <$1.0 ms;
4) prompt-delayed distance cut $R_{\rm p-d}$ <1.5 m;

Finally, we can get that the accidental background rate in the fiducial volume is nearly 1.1/day. This is acceptable compared with the expected signal rate of 60/day for IBD.

5 Conclusion

The JUNO experiment is designed to operate with very low radioactivity backgrounds. From the Geant4 simulation results, we know that when the buffer thickness between PMT and LS is 1.5 m, the buffer thickness between rock and LS is 3.2 m, the requirements for radiopurity of materials in the JUNO detector are as shown in Table 1 and Table 3, and the LS fiducial volume radius is cut from 17.7 m to 17.2 m, the accidental background induced by natural radioactivity in the JUNO central detector is 1.1/day, which is 1.8% of the expected IBD signal events (60/day). The results of the present study will provide an important basis for optimization of the JUNO design.

The authors thank members of the JUNO central detector group for their valuable discussions, and sincerely thank Xiaoyan Ma, Xiaohui Qian, and Jiajun Hao for their help on the PMT arrangement.

References

1 Y. F. Li, J. Cao, Y. Wang, and L. Zhan, Phys. Rev. D, **88**: 013008 (2013)
2 K. Eguchi et al (KamLAND Collaboration), Phys. Rev. Lett., **90**: 021802 (2003)
3 M. Apollonio et al (CHOOZ Collaboration), Eur. Phys. J. C, **27**: 331 (2003)
4 C. Arpesella et al (Borexino Collaboration), Phys. Lett. B, **658**: 101 (2008)
5 F. P. An et al (Daya Bay Collaboration), Phys. Rev. Lett., **108**: 171803 (2012)
6 Y. Abe et al (Double Chooz Collaboration), Phys. Rev. Lett., **108**: 131801 (2012)
7 J. K. Ahn et al (RENO Collaboration), Phys. Rev. Lett., **108**: 191802 (2012)
8 S. Agostinelli et al (GEANT4 Collaboration), Nucl. Instrum. Methods A, **506**: 250 (2003)
9 http://www.us.schott.com/english/index.html
10 http://www.nndc.bnl.gov/ensdf/
11 M. Motoki, F. Suekane, K. Tada and Y. Tsuda, Nucl. Instrum. Methods A, **534**: 59 (2004)
12 http://sno.phy.queensu.ca/sno/str/SNO-STR-92-061.pdf, retrieved 17th September 1992
13 J. Su et al (CDEX Collaboration), Chin. Phys. C, **39**(3): 036001 (2015)